

Evolution of shell gaps in the neutron-poor calcium region from invariant-mass spectroscopy of $^{37,38}\text{Sc}$, ^{35}Ca , and ^{34}K

N. Dronchi^{1,*}, R. J. Charity², L. G. Sobotka^{1,2}, B. A. Brown^{1,3,4}, D. Weisshaar¹, A. Gade^{1,3,4}, K. W. Brown^{1,3,5}, W. Reviol¹, D. Bazin^{1,3,4}, P. J. Farris^{3,4}, A. M. Hill^{1,3,4}, J. Li³, B. Longfellow^{3,4}, D. Rhodes^{3,4}, S. N. Paneru³, S. A. Gillespie¹, A. K. Anthony¹, E. Rubino³, and S. Biswas³

¹Department of Physics, Washington University, St. Louis, Missouri 63130, USA

²Department of Chemistry, Washington University, St. Louis, Missouri 63130, USA

³Facility for Rare Isotope Beams, Michigan State University, East Lansing, Michigan 48824, USA

⁴Department of Physics and Astronomy, Michigan State University, East Lansing, Michigan 48824, USA

⁵Department of Chemistry, Michigan State University, East Lansing, Michigan 48824, USA

⁶Physics Division, Argonne National Laboratory, Argonne, Illinois 60439, USA



(Received 31 May 2024; accepted 13 August 2024; published 12 September 2024)

A fast secondary beam of ^{37}Ca impinged on a ^9Be target resulting in a set of reactions populating proton-rich nuclei including ^{35}Ca and the first observations of $^{37,38}\text{Sc}$ and ^{34}K . Invariant-mass spectroscopy, used to reconstruct proton decays for these nuclei, yielded three new ground-state masses and information on their low-lying structures. The newly measured mass excesses are: $\Delta M(^{37}\text{Sc}) = 3500(410)$ keV, $\Delta M(^{38}\text{Sc}) = -4656(14)$ keV, and $\Delta M(^{34}\text{K}) = -1487(17)$ keV. These nuclei straddle the well-known $Z = 20$ shell closure as well as the $N = 16$ subshell closure. Trends in separation energies help elucidate how nuclear structure evolves showing a fading of the $Z = 20$ shell gap for $N \leq 18$ and indications of a $N = 16$ subshell gap.

DOI: [10.1103/PhysRevC.110.L031302](https://doi.org/10.1103/PhysRevC.110.L031302)

Introduction. The magic numbers (2, 8, 20, 28, 50, 82, and 126) arise as a result of the shape of the attractive nuclear interaction and spin-orbit coupling creating energy gaps between shells for protons and neutrons [1]. These magic numbers help explain the natural abundances of isotopes in nature, the large number of stable isotopes or isotones with magic numbers of protons or neutrons, trends in nuclear masses, and the double-humped mass distribution observed in fission.

Away from stability, the picture of shell closures changes as the classic shell gaps known at stability weaken and new subshell closures appear. The disappearance of the $N = 20$ closed shell is manifested in ^{32}Mg by occupation of the $\nu 0f_{7/2}$ intruder orbit in the ground state. This effect leads to a region of the chart of the nuclides called the island of inversion [2,3]. At $Z = 14$ and $N = 20$, ^{34}Si was shown to be doubly magic and potentially a proton bubble nucleus [4]. In the oxygen isotopes, the $N = 16$ subshell closure is observed at ^{24}O [5] with a gap between the $\nu 1s_{1/2}$ and $\nu 0d_{3/2}$ orbits while the $N = 20$ shell closure is not observed in ^{28}O [6]. These effects are driven by the monopole component of the nuclear interaction, which has central, tensor, two-body spin-orbit, and three-nucleon components [7,8].

Mass measurements for neutron-rich calcium isotopes have provided evidence for shell closures at both $N = 32$ and $N = 34$ [9,10]. For proton-rich Ca isotopes, a subshell closure at $N = 16$ has also been suggested [11]. These claims arise from

a large value for the change in neutron separation energy, ΔS_n . Evidence for the weakening of the standard $Z = 20$ shell is found in the apparent need for cross-shell proton excitations to explain the measured $B(E2 \uparrow)$ value and two-neutron removal cross sections for neutron-deficient ^{36}Ca and ^{38}Ca [12,13]. The present work further illuminates the shell gaps in this region through mass measurements of proton unbound isotopes.

Methods. At the National Superconducting Cyclotron Laboratory, a secondary beam of ^{37}Ca was produced at 72 MeV/A with a purity of 40%. This work only considers reactions from ^{37}Ca projectiles. This beam impinged on a 0.5-mm-thick Be target resulting in multinucleon knockout, proton pickup, and charge exchange reactions. The reaction products were detected with a setup including the CAESAR array [14], a Si-CsI(Tl) $\Delta E - E$ Ring Telescope (RT), a Scintillating-Fiber Array (SFA), and the S800 Spectrograph [15]. Further detail on the experimental setup can be found in Ref. [12].

Invariant mass fits. Total decay-energy (E_T) spectra were measured using the invariant-mass method. The E_T spectra were typically fit with multiple peaks sitting upon a background. The peaks were assumed to have zero intrinsic decay width as most states were predicted with shell model calculations (see later) to have intrinsic widths less than 1 keV while the experimental resolution is roughly two orders of magnitude larger. The lineshape due to the detector resolution and acceptance is calculated from Monte Carlo simulations and binned to match that of the experiment [16]. At larger E_T , typically around 2 MeV, the simulated peak shape flattens as the efficiency drops for transverse decays (decay axis

*Contact author: n.dronchi@wustl.edu

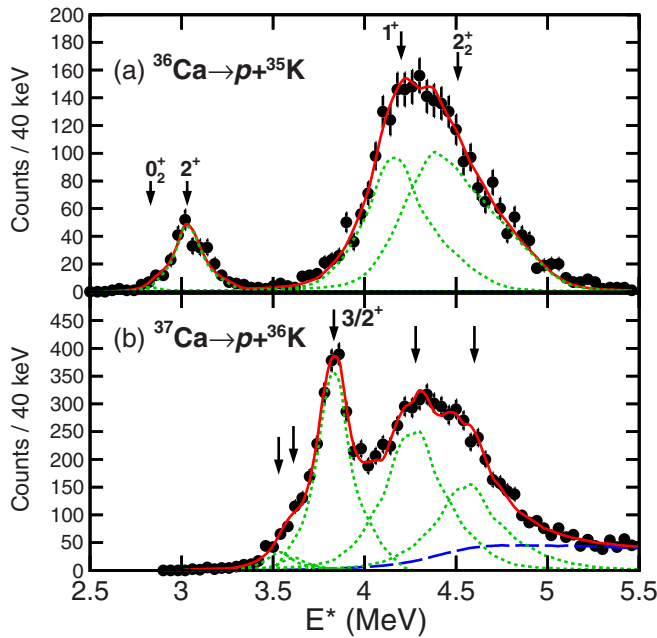


FIG. 1. Data points show the excitation-energy spectra of (a) ^{36}Ca from the invariant-mass of $p + ^{35}\text{K}$ events and (b) ^{37}Ca from $p + ^{36}\text{K}$ events. The red curves are from fits with multiple peaks each shown by the green dotted curves. No background was needed in fitting the ^{36}Ca data while the blue-dashed line in (b) indicates the background for the ^{37}Ca fit. Arrows indicate states included in the fits. The two states below the $3/2^+$ level in (b) are fixed to the energies of states found in the γ -decay studies [20], while the states above the $3/2^+$ state have not been previously observed.

perpendicular to the beam axis) as such events miss the RT and only longitudinal decays remain. Longitudinal decays have worse decay-energy resolution than transverse decays, resulting in flatter experimental and simulated peaks [16,17]. Backgrounds for the ^{35}Ca , ^{37}Ca , and ^{34}K data were included via event mixing with the procedure developed previously for knockout reactions [18]. Backgrounds in the data for $^{37,38}\text{Sc}$ are discussed in the results section.

Our invariant-mass resolution was exemplified by two states studied previously, see Fig. 1. The 2^+ state in ^{36}Ca has been measured multiple times through in-beam γ spectroscopy and the resulting weighted average excitation energy is $E^* = 3.0459(18)$ MeV [12,19–21]. The value from the present study, see Fig. 1(a), is $E^* = 3.031$ MeV with a 8 keV statistical uncertainty from the fit and a 5.6 keV uncertainty in the employed mass of ^{36}Ca [22]. In the present work, the second 0^+ state in ^{36}Ca is very weakly populated and its energy is fixed in the fit. The excitation of the $3/2^+$ state in ^{37}Ca has $E^* = 3.842(4)$ MeV determined by in-beam γ spectroscopy [20]. We find this state, see Fig. 1(b), at $E^* = 3.833$ MeV with a 4 keV statistical uncertainty. Using these two states, we estimate the systematic uncertainty to be approximately 10 keV. For the overall uncertainties reported in this work we add this estimate in quadrature with the fitted statistical uncertainties.

Results for ^{35}Ca and ^{34}K . The ground state of ^{35}Ca is particle bound with a mass excess $\Delta M = 4777(105)$ keV [11].

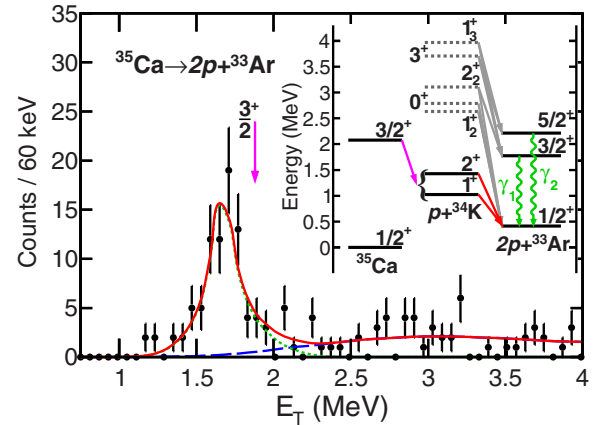


FIG. 2. Total decay-energy spectrum for two-proton emitting states in ^{35}Ca with a single peak fit (line type and colors same as Fig. 1). The USDC shell-model decay energy for the $3/2^+$ state is shown by the magenta arrow. The insert shows the decay scheme for ^{35}Ca through ^{34}K with the magenta, red, and green arrows matching decays from states seen here and in Fig. 3.

The first excited state, predicted to be $J^\pi = 3/2^+$, is unbound to both $1p$ decay to ^{34}K and $2p$ decay to ^{33}Ar . Because ^{34}K is unbound, the first excited state will only appear in the $2p + ^{33}\text{Ar}$ exit channel. The $2p + ^{33}\text{Ar}$ decay-energy spectrum is shown in Fig. 2 along with a fit to a single peak at $E_T = 1.667(20)$ MeV. The region above 2 MeV is fit with an event mixing background but could also be fit with a peak around 2.8 MeV.

Data for the first observation of ^{34}K is presented in Fig. 3 showing the decay-energy spectrum for $p + ^{33}\text{Ar}$ events. The spectrum has two sharp resonances at $E_T = 0.608(17)$ and $1.009(18)$ MeV. The latter corresponds to an excitation energy of $E^* = 0.401(25)$, presuming the lower-energy peak is the

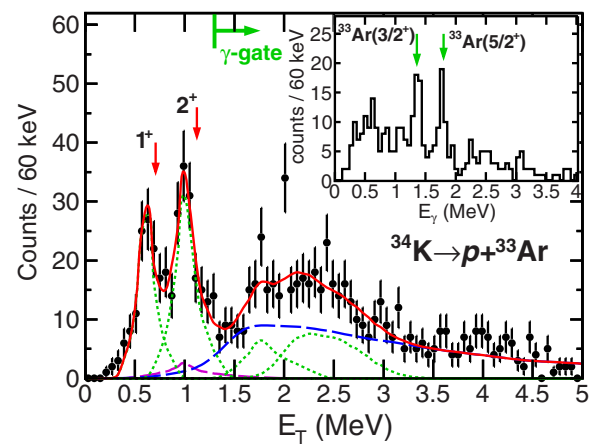


FIG. 3. Total decay-energy spectrum for ^{34}K fitted with four peaks (line colors same as Fig. 1). A small contribution from $^{35}\text{Ca} \rightarrow 2p + ^{33}\text{Ar}$ events missing a proton is included (magenta dashed line). Red arrows indicate the predicted ground and first excited states from USDC shell-model calculations. The inset shows the γ -ray energy spectrum in coincidence with $p + ^{33}\text{Ar}$ events having $E_T > 1.36$ MeV.

ground state. At low relative energies, there is possible contamination from ^{35}Ca decays where the first emitted proton is detected but the second is missed. Assuming sequential $2p$ decay, the observed population of ^{35}Ca excited state was used along with the simulated efficiencies for detecting the first but not the second proton, resulting in a very small contribution shown by the magenta dashed curve under the second peak.

Above a decay energy of 1.5 MeV, the spectrum could be fit with multiple levels, but a two peak fit offered the fewest number of states that could reasonably reproduce the data. The peaks at $E_T = 1.85$ MeV and 2.42 MeV sit on the large background determined though event mixing. The correlation function used to weight the mixed events in the procedure of [18] could not be uniquely determined in this experiment so the $^3\text{He} + ^8\text{B}$ correlation from Ref. [18] was used instead. A gate requiring $E_T > 1.36$ MeV was applied to look for γ decays in coincidence with $p + ^{33}\text{Ar}$ events. The result, shown as an insert in Fig. 3, indicates that the $J^\pi = 3/2^+$ and $J^\pi = 5/2^+$ states in ^{33}Ar are populated after proton decay. This suggests, but does not prove due to the significant background, that the E_T region above 1.36 MeV contains some highly excited states in ^{34}K that proton decay to γ -decaying excited states in ^{33}Ar .

Shell-model calculations using the USDC Hamiltonian [23] were used to assign spins and parities of the states observed in ^{35}Ca and ^{34}K . The USDC Hamiltonian is the latest iteration of universal sd shell Hamiltonians that incorporate Coulomb and other isospin-breaking interactions which can become important at and beyond the drip-line. Starting with ^{35}Ca , the magenta arrow in Fig. 2 indicates the predicted decay energy of $E_T = 1.880$ MeV. This is 213 keV higher than observed, but this predicted value depends on the mass of ^{33}Ar , which is overbound in the calculation by 277 keV compared to AME2020 [24]. This calculation predicts that the $^{35}\text{Ca}(3/2^+)$ state proton decays primarily through the $^{34}\text{K}(1^+)$ ground state, a prediction that we do not have sufficient statistics to confirm.

The USDC calculations for ^{34}K again predict energies slightly higher than measured, $E_T = 0.708$ MeV (versus 0.608 MeV measured) for the 1^+ ground state and $E_T = 1.123$ MeV (versus 1.009 MeV measured) for the 2^+ first excited state, see red arrows in Fig. 3. The spacing and order of the 1^+ and 2^+ states agree with what is observed in the mirror nucleus ^{34}P . The calculations also predict many states between 1.36 MeV and 3 MeV, some, like 1_2^+ and 0^+ , that decay to the ground state of ^{33}Ar and others, like 2_2^+ , 3^+ , and 1_3^+ , that have decay branches to excited states of ^{33}Ar . These predicted states and their decays are included as gray dotted lines and arrows in the decay scheme of Fig. 2. In addition there are negative parity states starting at 2.3 MeV in ^{34}P which should also occur in ^{34}K but are not part of the USDC calculations. The present data cannot resolve these possible states.

Results for ^{37}Sc and ^{38}Sc . Charge exchange reactions produced a small number of ^{37}Sc events observed to proton decay to ^{36}Ca . These data, shown in Fig. 4, were fit with either one or two peaks plus an extra wide peak at $E_T = 5$ MeV acting as a background. The single peak fit, shown in Fig. 4(a), suggests $E_T = 3.00(5)$ MeV, but this fit misses the data points to either

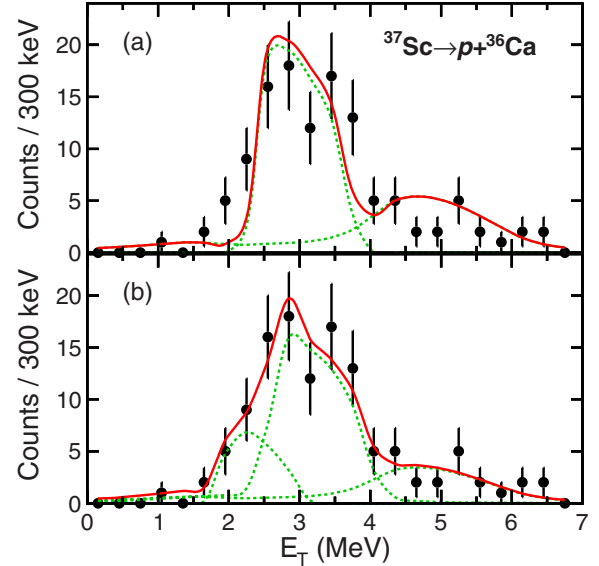


FIG. 4. Total decay-energy spectrum for ^{37}Sc . (a) Shows a one-peak fit while (b) shows a two-peak fit (line colors same as Fig. 1). The high-energy structure near 5 MeV is fit with a peak but is considered to be the background contribution.

side of the peak. The fit is potentially remedied if the ground state has a large intrinsic width of ≈ 600 keV, but this is not supported by the shell-model predictions. The two peak fit, shown in Fig. 4(b), finds states at $E_T = 2.37(13)$ MeV and $E_T = 3.24(8)$ MeV.

The mirror nucleus, ^{37}S has a $7/2^-$ ground state with a $3/2^-$ state at 0.646 MeV [25]. In ^{37}Sc the Thomas-Ehrman shift of the $3/2^-$ ($1p_{3/2}$) will lower its energy. The Thomas-Ehrman shift observed for the $3/2^-$ excited states in ^{41}Sc and ^{41}Ca is 0.23 MeV. So a fit with two low-lying states in ^{37}Sc is expected. In addition there is a $3/2^+$ state at 1.398 MeV in ^{37}S which could account for a third peak around $E_T = 4.5$ MeV in ^{37}Sc . The amount of data and the resolution are insufficient to make definitive statements. Nevertheless, this nuclide is observed and a ground-state mass estimate is obtained where the uncertainty encompasses the results from both fits (see Table I).

The data for the first observation of ^{38}Sc is presented in Fig. 5 where the decay-energy spectrum for $p + ^{37}\text{Ca}$ events is shown. The spectrum shows a resolved state (ground state) at $E_T = 1.191(14)$ MeV. A second peak at $E_T = 1.823(16)$ MeV [$E^* = 0.632(22)$ MeV] is well constrained from the sharp rise but at higher energy, blends into a region where the resolution declines. A third peak, at $E_T = 2.40$ MeV, is required for an acceptable fit, but is not well constrained. The background contribution is fit with an inverse Fermi function multiplied by a decreasing linear function to give the required smooth increase and a long tail. It is also possible that the data has contributions from more states such as those seen in the mirror ^{38}Cl . These states come from the $3/2^+$ ground state of ^{37}Ca (^{37}Cl) coupling with the $0f_{7/2}$ proton (neutron) to make $J^\pi = (2, 3, 4, 5)^-$. The 0.63 MeV spacing of the first two peaks in Fig. 5 is consistent with the

TABLE I. Parameters of states identified in this work. Excitation energies and mass excesses are relative to masses from the AME2020 [24] except for ^{35}Ca [11] and ^{36}Ca [22]. States reported without uncertainties were not well constrained by their fits.

Nuclide	J^π	E_T (MeV)	E^* (MeV)	ΔM (keV)
^{34}K	1^+	0.608(17)	g.s.	-1487(17)
	2^+	1.009(18)	0.401(25)	
		≈ 1.85	≈ 1.24	
		≈ 2.42	≈ 1.81	
^{35}Ca	$3/2^+$	1.667(20)	2.08(10)	
^{36}Ca	2^+	0.464(13)	3.031(14)	
	1^+	1.632(15)	4.199(18)	
	2^+	≈ 1.94	≈ 4.51	
^{37}Ca	$3/2^+$	0.825(11)	3.833(11)	
		1.271(15)	4.279(15)	
		≈ 1.60	≈ 4.60	
^{37}Sc	$7/2^-$	2.69(41)	g.s.	3500(410)
^{38}Sc	2^-	1.191(14)	g.s.	-4656(14)
	(3^- or 5^-)	1.823(16)	0.632(22)	
		≈ 2.40	≈ 1.21	

spacing of 0.67 MeV between the 2^- ground state and the 5^- first excited state of ^{38}Cl . A fit with an extra state with the spacing between the 2^- and 3^- states in ^{38}Cl is also consistent with these data.

Analysis. A summary of the states measured is provided in Table I. The mass measurements prompt a reexamination of the trends in neutron and proton separation energies as the former can be extended for potassium isotopes down to $N = 16$ and the latter extended for $N = 16$ and $N = 17$ isotones up to scandium.

The trends in neutron separation energy are shown in Fig. 6(a), while Fig. 6(b) plots the change in neutron separation energy between isotopes given by $\Delta S_n(N, Z) = S_n(N, Z) - S_n(N + 1, Z) = \Delta M(N + 1, Z) - 2\Delta M(N, Z) + \Delta M(N - 1, Z)$. The change in proton separation energy, $\Delta S_p(N, Z)$, is similarly defined and is plotted along with proton separation energies in Figs. 7(a) and 7(b). Figures 6 and 7 show the new data enabled by the present work as stars. The jumps in ΔS_n at $N = 20$ and

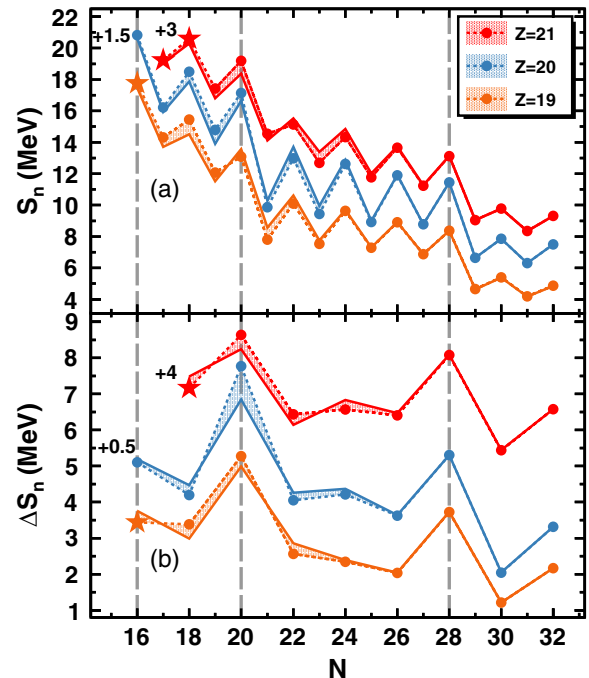


FIG. 6. (a) Experimental neutron separation energies for Sc, Ca, and K isotopes. (b) Changes in neutron separation energies for even N isotopes. Data are represented by points (or stars for new values) connected by dashed lines and are shifted up as indicated. Removing the Wigner energy results in the solid lines which show an increase in neutron separation energy at $N = 16$ for $Z = 19$ resembling that seen for $Z = 20$.

$N = 28$ illustrate the classic shell closures. The increase in ΔS_n at $N = 32$ indicates an increased stability at this subshell closure.

At $N = 16$, the raw data (points connected with dotted lines) might suggest a neutron shell closure for ^{36}Ca as was argued in Ref. [11] where the increase in ΔS_n from $N = 18$ to $N = 16$ was noted for $Z = 20$ (blue data). However, for $Z = 19$ (orange data), this increase has largely diminished. For experimental data in this region, shell effects are conflated with the Wigner energy, where isotopes near $N = Z$ have large $T = 0$ neutron-proton pairing correlations that increase the binding energy [26]. Removing the Wigner energy from the separation energies using the form suggested by Goriely *et al.* [27], results in the solid lines in Figs. 6 and 7. The shading between the solid and dashed lines highlights the Wigner energy contribution. The Wigner-removed separation energies show the effect of the $N = 16$ subshell closure is also present for potassium isotopes with an increase from $N = 18$ to $N = 16$ similar to that seen for calcium isotopes.

Using a similar logic, the $Z = 20$ shell gap was investigated following proton separation energies across an isotone chain. The proton separation energy differences for isotones between $N = 20$ and $N = 16$ are shown in Fig. 7(b). The $Z = 14$ subshell closure is most clearly seen as a peak in ΔS_p between $N = 17$ and $N = 20$. At $N = 16$, there is no evidence for this feature. With 16 neutrons, the $v0d_{5/2}$ and $v1s_{1/2}$ orbitals are nominally filled, so adding another neutron

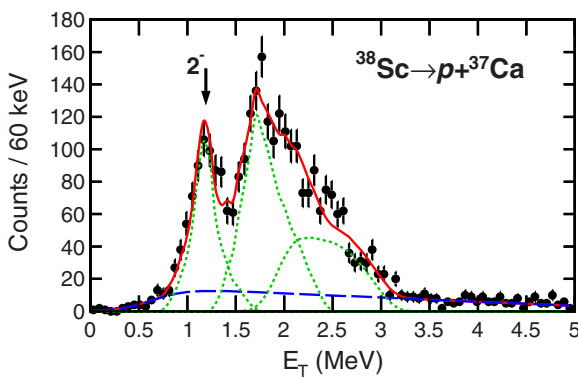


FIG. 5. Total decay-energy spectrum for ^{38}Sc is shown with a three-peak fit (line colors same as Fig. 1).

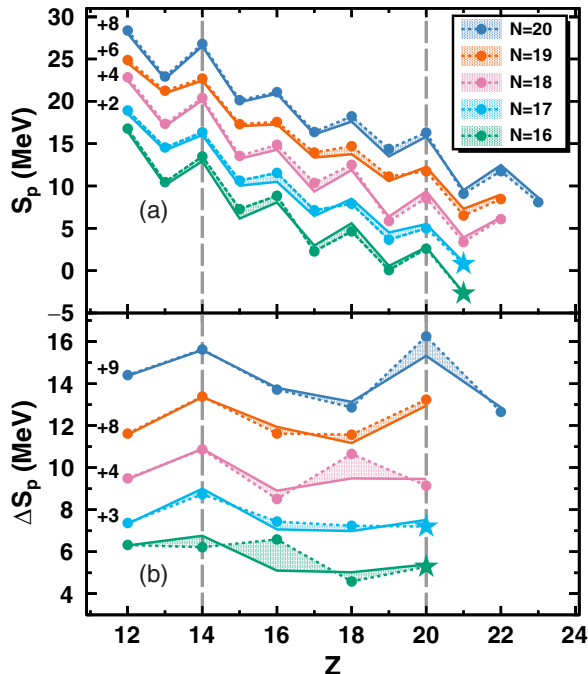


FIG. 7. (a) Proton separation energies for isotones from $16 \leq N \leq 20$. (b) Changes in proton separation energies for even Z isotones. Data are represented by points (or stars for new values) connected by dashed lines and are shifted up as indicated. Removing the Wigner energy results in the solid lines which show the trends for $Z = 14$ and $Z = 20$.

starts filling the $\nu 0d_{3/2}$ orbital. Through the tensor interaction [7], neutrons occupying the $\nu 0d_{3/2}$ will stabilize the $\pi 0d_{5/2}$, increasing the energy gap between it and the $\pi 1s_{1/2}$. This effect explains the observed low proton occupation of the $\pi 1s_{1/2}$ orbit in ^{34}Si , leading to the conclusion that this nucleus is doubly magic [4].

The nucleus ^{40}Ca is doubly magic with $N = Z = 20$. Here, the $Z = 20$ shell closure appears as a sharp drop in S_p when adding a proton to get ^{41}Sc . Looking at the Wigner-removed separation energies, the $N = 19$ isotones show a similar increase in stability but the mass of ^{43}V has not been measured, so a point at $\Delta S_p(N = 19, Z = 22)$ cannot be determined. For the neutron deficient calcium isotopes, the $Z = 20$ shell closure weakens markedly at $N = 18$. The Wigner-removed

energies show no jump at $N = 18$ and the data from the present work, see stars for ^{38}Sc and ^{37}Sc , verify that there is little to no increased stability at $Z = 20$ for $N = 17$ and $N = 16$.

Conclusion. Using invariant-mass spectroscopy, previously unknown proton decays near or beyond the proton drip-line were observed. The $3/2^+$ first excited state of ^{35}Ca was observed and provides an update to the excitation energy for this state. This work presents the first observations of $^{37,38}\text{Sc}$ and ^{34}K all of which are odd- Z ground-state single-proton emitters. The data for ^{34}K was fit to determine the ground-state mass as well as the energy of the first excited state. Higher-lying states in ^{34}K were not resolved, but there is evidence that they decay to excited states of ^{33}Ar . The data for ^{37}Sc were sparse but provided a ground-state-mass measurement with a relatively large uncertainty. In addition, the ground-state mass and energy of the first excited state of ^{38}Sc were measured. Comparisons of the resolved states with predictions from the USDC shell-model Hamiltonian show agreement with the data.

The ground-state masses measured in this work were used to examine trends in proton and neutron separation energies. The $N = 16$ subshell closure was investigated through neutron separation energies in the potassium isotopic chain, showing signs of increased stability in ^{35}K when the Wigner energy is removed. Removing this neutron-proton $T = 1$ (but not necessarily $J = 1$) congruence stabilization energy is crucial to understanding how shells evolve close to $N = Z$ [28]. The proton separation energies show a weakening of the $Z = 20$ shell closure in this neutron deficient region. This is in agreement with the analysis of the $^{36}\text{Ca} B(E2 \uparrow)$ strength [12] and the two-nucleon removal cross section for ^{38}Ca [13]. This has also been mentioned in a recent global examination of the trends in shell gaps over the whole chart of nuclides [28]. The three masses measured in this work help understand the evolution of shells in nuclei far from stability.

Acknowledgments. This material is based upon work supported by the U.S. Department of Energy, Office of Science, Office of Nuclear Physics under Awards No. DE-FG02-87ER-40316 (WU), DE-SC0020451, and DE-SC0023633 (MSU) and Contract No. DE-AC02-06CH11357 (ANL), and by the U.S. National Science Foundation (NSF) under Grants No. PHY-1565546 and PHY-2110365, and by the DOE National Nuclear Security Administration through the Nuclear Science and Security Consortium, under Award No. DE-NA0003180.

- [1] M. G. Mayer, *Phys. Rev.* **75**, 1969 (1949).
- [2] T. Motobayashi, Y. Ikeda, K. Ieki, M. Inoue, N. Iwasa, T. Kikuchi, M. Kurokawa, S. Moriya, S. Ogawa, H. Murakami, S. Shimoura, Y. Yanagisawa, T. Nakamura, Y. Watanabe, M. Ishihara, T. Teranishi, H. Okuno, and R. Casten, *Phys. Lett. B* **346**, 9 (1995).
- [3] A. Ozawa, T. Kobayashi, T. Suzuki, K. Yoshida, and I. Tanihata, *Phys. Rev. Lett.* **84**, 5493 (2000).
- [4] A. Mutschler, A. Lemasson, O. Sorlin, D. Bazin, C. Borcea, R. Borcea, Z. Dombrádi, J.-P. Ebran, A. Gade, H. Iwasaki, E. Khan, A. Lepailleur, F. Recchia, T. Roger, F. Rotaru, D. Sohler, M. Stanoiu, S. R. Stroberg, J. A. Tostevin, M. Vandebrouck *et al.*, *Nat. Phys.* **13**, 152 (2017).
- [5] C. R. Hoffman, T. Baumann, D. Bazin, J. Brown, G. Christian, D. H. Denby, P. A. DeYoung, J. E. Finck, N. Frank, J. Hinnefeld, S. Mosby, W. A. Peters, W. F. Rogers, A. Schiller, A. Spyrou, M. J. Scott, S. L. Tabor, M. Thoennessen, and P. Voss, *Phys. Lett. B* **672**, 17 (2009).
- [6] Y. Kondo, N. L. Achouri, H. A. Falou, L. Atar, T. Aumann, H. Baba, K. Boretzky, C. Caesar, D. Calvet, H. Chae, N. Chiga,

- A. Corsi, F. Delaunay, A. Delbart, Q. Deshayes, Z. Dombrádi, C. A. Douma, A. Ekström, Z. Elekes, C. Forssén *et al.*, *Nature (London)* **620**, 965 (2023).
- [7] T. Otsuka, R. Fujimoto, Y. Utsuno, B. A. Brown, M. Honma, and T. Mizusaki, *Phys. Rev. Lett.* **87**, 082502 (2001).
- [8] T. Otsuka, A. Gade, O. Sorlin, T. Suzuki, and Y. Utsuno, *Rev. Mod. Phys.* **92**, 015002 (2020).
- [9] F. Wienholtz, D. Beck, K. Blaum, C. Borgmann, M. Breitenfeldt, R. B. Cakirli, S. George, F. Herfurth, J. D. Holt, M. Kowalska, S. Kreim, D. Lunney, V. Manea, J. Menéndez, D. Neidherr, M. Rosenbusch, L. Schweikhard, A. Schwenk, J. Simonis, J. Stanja *et al.*, *Nature (London)* **498**, 346 (2013).
- [10] S. Michimasa, M. Kobayashi, Y. Kiyokawa, S. Ota, D. S. Ahn, H. Baba, G. P. A. Berg, M. Dozono, N. Fukuda, T. Furuno, E. Ideguchi, N. Inabe, T. Kawabata, S. Kawase, K. Kisamori, K. Kobayashi, T. Kubo, Y. Kubota, C. S. Lee, M. Matsushita *et al.*, *Phys. Rev. Lett.* **121**, 022506 (2018).
- [11] L. Lalanne, O. Sorlin, A. Poves, M. Assié, F. Hammache, S. Koyama, D. Suzuki, F. Flavigny, V. Girard-Alcindor, A. Lemasson, A. Matta, T. Roger, D. Beaumel, Y. Blumenfeld, B. A. Brown, F. D. O. Santos, F. Delaunay, N. de Sérerville, S. Franschoo, J. Gibelin *et al.*, *Phys. Rev. Lett.* **131**, 092501 (2023).
- [12] N. Dronchi, D. Weisshaar, B. A. Brown, A. Gade, R. J. Charity, L. G. Sobotka, K. W. Brown, W. Reviol, D. Bazin, P. J. Farris, A. M. Hill, J. Li, B. Longfellow, D. Rhodes, S. N. Paneru, S. A. Gillespie, A. Anthony, E. Rubino, and S. Biswas, *Phys. Rev. C* **107**, 034306 (2023).
- [13] T. Beck, A. Gade, B. A. Brown, J. A. Tostevin, D. Weisshaar, D. Bazin, K. W. Brown, R. J. Charity, P. J. Farris, S. A. Gillespie, A. M. Hill, J. Li, B. Longfellow, W. Reviol, and D. Rhodes, *Phys. Rev. C* **108**, L061301 (2023).
- [14] D. Weisshaar, A. Gade, T. Glasmacher, G. F. Grinyer, D. Bazin, P. Adrich, T. Baugher, J. M. Cook, C. A. Diget, S. McDaniel, A. Ratkiewicz, K. P. Siwek, and K. A. Walsh, *Nucl. Instrum. Methods Phys. Res. A* **624**, 615 (2010).
- [15] J. Yurkon, D. Bazin, W. Benenson, D. Morrissey, B. Sherrill, D. Swan, and R. Swanson, *Nucl. Instrum. Methods Phys. Res. A* **422**, 291 (1999).
- [16] R. J. Charity, K. W. Brown, J. Elson, W. Reviol, L. G. Sobotka, W. W. Buhro, Z. Chajecki, W. G. Lynch, J. Manfredi, R. Shane, R. H. Showalter, M. B. Tsang, D. Weisshaar, J. R. Winkelbauer, S. Bedoor, and A. H. Wuosmaa, *Phys. Rev. C* **99**, 044304 (2019).
- [17] R. J. Charity, K. W. Brown, J. Okołowicz, M. Płoszajczak, J. M. Elson, W. Reviol, L. G. Sobotka, W. W. Buhro, Z. Chajecki, W. G. Lynch, J. Manfredi, R. Shane, R. H. Showalter, M. B. Tsang, D. Weisshaar, J. R. Winkelbauer, S. Bedoor, and A. H. Wuosmaa, *Phys. Rev. C* **100**, 064305 (2019).
- [18] R. J. Charity and L. G. Sobotka, *Phys. Rev. C* **108**, 044318 (2023).
- [19] P. Doornenbal, P. Reiter, H. Grawe, T. Otsuka, A. Al-Khatib, A. Banu, T. Beck, F. Becker, P. Bednarczyk, G. Benzoni, A. Bracco, A. Bürger, L. Caceres, F. Camera, S. Chmel, F. C. Crespi, H. Geissel, J. Gerl, M. Górska, J. Grebosz *et al.*, *Phys. Lett. B* **647**, 237 (2007).
- [20] A. M. Amthor, Experimental and theoretical study of nuclear reaction rates in the RP-process, Ph.D thesis, Michigan State University, 2008.
- [21] A. Bürger, F. Azaiez, A. Algora, A. Al-Khatib, B. Bastin, G. Benzoni, R. Borcea, C. Bourgeois, P. Bringel, E. Clément, J.-C. Dalouzy, Z. Dlouhý, Z. Dombrádi, A. Drouart, C. Engelhardt, S. Franschoo, Z. Fülpö, A. Görgen, S. Grévy, H. Hübel *et al.*, *Phys. Rev. C* **86**, 064609 (2012).
- [22] J. Surbrook, G. Bollen, M. Brodeur, A. Hamaker, D. Pérez-Loureiro, D. Puentes, C. Nicoloff, M. Redshaw, R. Ringle, S. Schwarz, C. S. Sumithrarachchi, L. J. Sun, A. A. Valverde, A. C. C. Villari, C. Wrede, and I. T. Yandow, *Phys. Rev. C* **103**, 014323 (2021).
- [23] A. Magilligan and B. A. Brown, *Phys. Rev. C* **101**, 064312 (2020).
- [24] M. Wang, W. Huang, F. Kondev, G. Audi, and S. Naimi, *Chin. Phys. C* **45**, 030003 (2021).
- [25] J. Cameron, J. Chen, B. Singh, and N. Nica, *Nucl. Data Sheets* **113**, 365 (2012).
- [26] W. Satuła, D. Dean, J. Gary, S. Mizutori, and W. Nazarewicz, *Phys. Lett. B* **407**, 103 (1997).
- [27] S. Goriely, N. Chamel, and J. M. Pearson, *Phys. Rev. C* **88**, 024308 (2013).
- [28] L. Buskirk, K. Godbey, W. Nazarewicz, and W. Satuła, *Phys. Rev. C* **109**, 044311 (2024).